Electronic Supplementary Information

Targeted synthesis of ionic liquid-polyoxometalates derived Mo-based electrodes for advanced electrochemical performance

Guojian Chen,*[a] Lei Zhang,[b] Yadong Zhang,[a] Ke Liu,[a] Zhouyang Long[a] and Ying Wang*[a]

[a] School of Chemistry and Materials Science, Jiangsu Key Laboratory of Green Synthetic Chemistry for Functional Materials, Jiangsu Normal University, Xuzhou 221116, China

[b] Centre for Clean Environment and Energy, Griffith University, Queensland 4222, Australia

E-mail: gjchen@jsnu.edu.cn (G. Chen); yingwang@jsnu.edu.cn (Y. Wang)

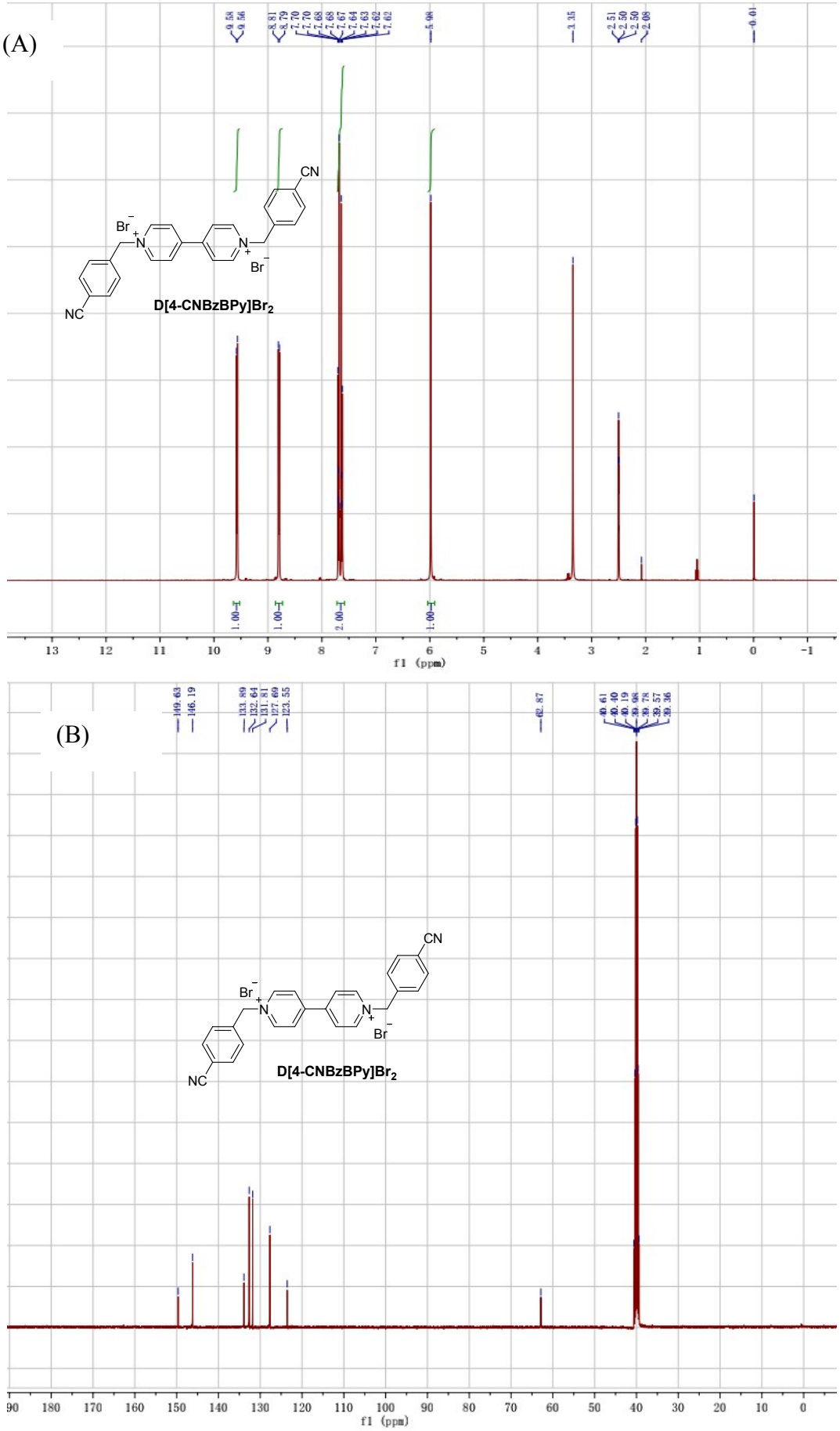

Fig. S1 (A) ^{1}HNMR and (B) ^{13}C NMR of D[4-CNBzBPy]Br_2.

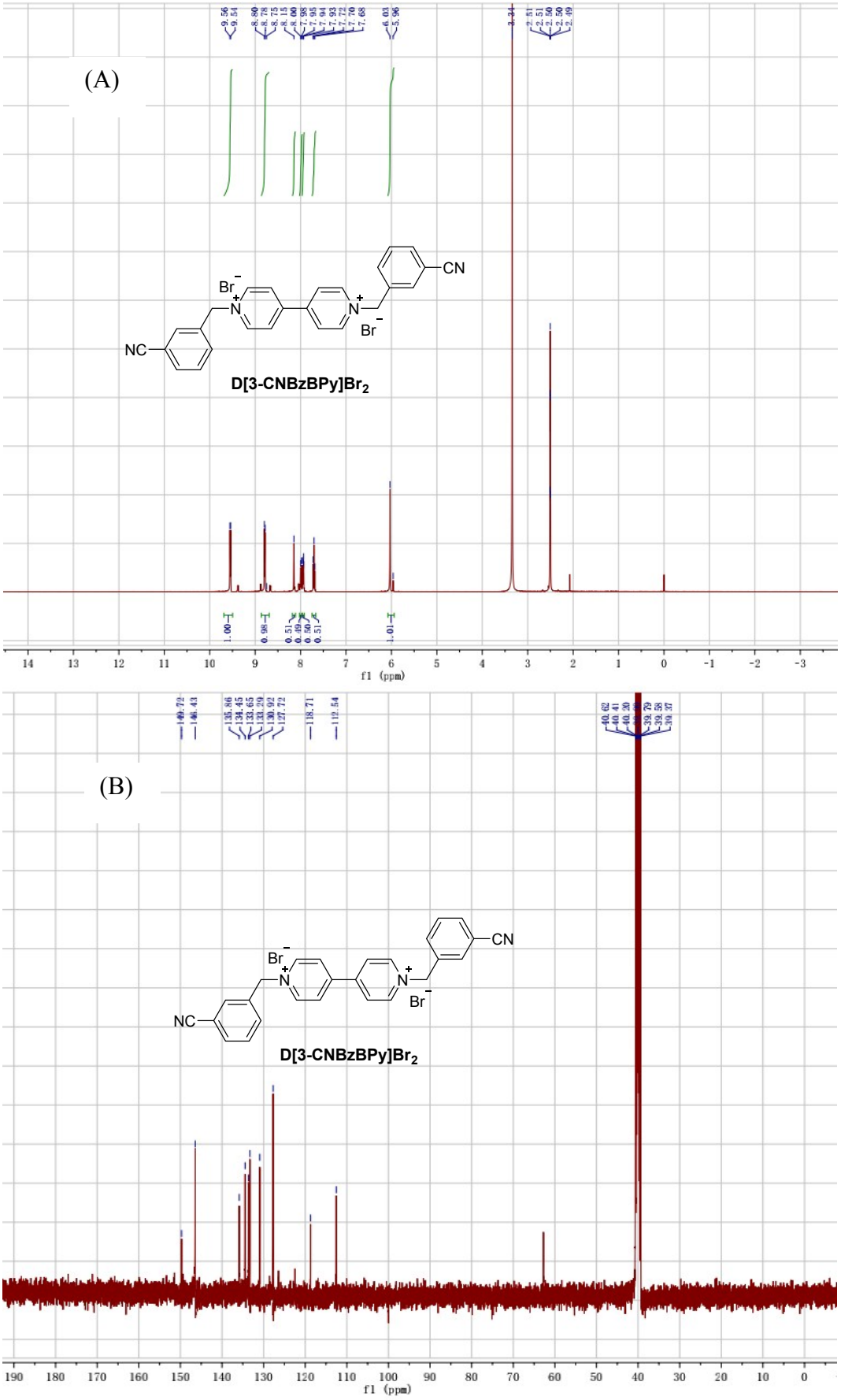

Fig. S2 (A) ^{1}HNMR and (B) ^{13}C NMR of D[3-CNBzBPy]Br_2.

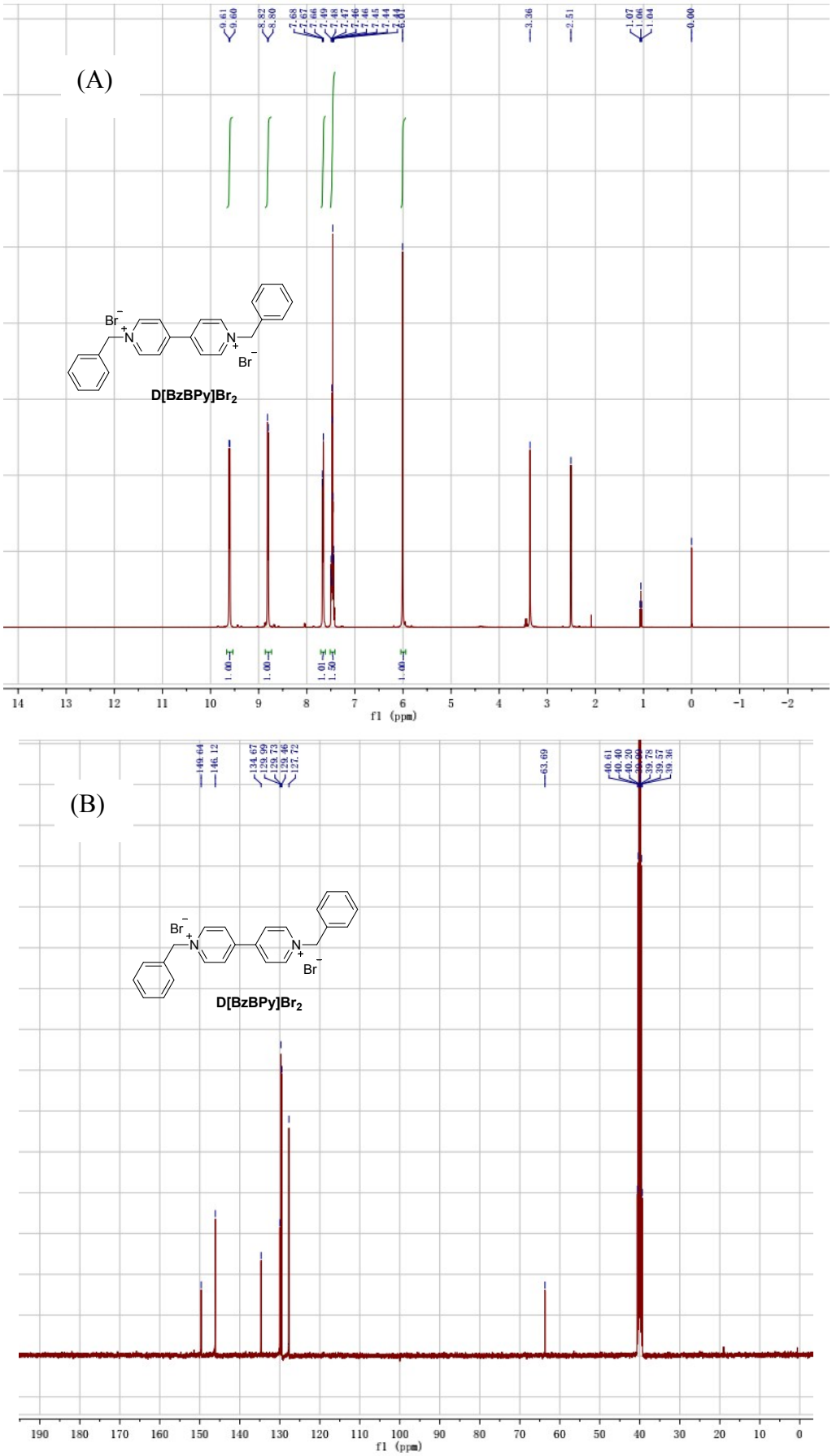

Fig. S3 (A) ^{1}HNMR and (B) ^{13}C NMR of D[BzBPy]Br_2.

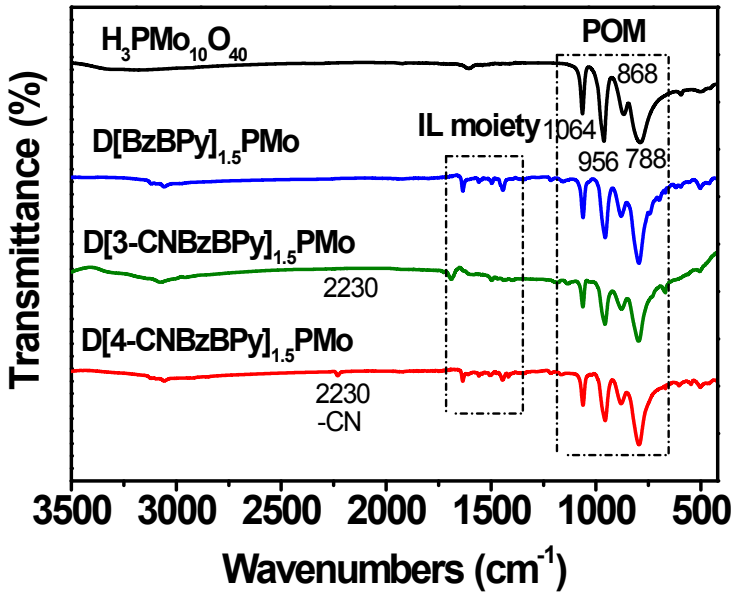

Fig. S4 FTIR spectra for the IL-POM hybrids and pure $H_3PMo_{12}O_{40}$.

Fig. S4 illustrates the FTIR spectra of pure $H_3PMo_{12}O_{40}$ and the three IL-POM hybrids. Four characteristic vibration bands for Keggin structure of $PMo_{12}O_{40}^{3-}$ anion are observed for $H_3PMo_{12}O_{40}$ at 1064, 956, 868 and 788 cm^{-1}, which assigned to the stretching vibration of the central oxygen $\nu(P\text{-}O_a)$, terminal oxygen $\nu(Mo{=}O_t)$, inter-octahedral oxygen $\nu(Mo\text{-}O_b\text{-}Mo)$, and intra-octahedral oxygen $\nu(Mo\text{-}O_c\text{-}Mo)$, respectively. After combined with viologen ionic liquid cations, the four Keggin featured bands for the formed IL-POM hybrids are also observed with only slight shifts, and the peaks located at 1635, 1497, 1445 cm^{-1} are assigned to the IL cations, and the weak peaks located at 2230 cm^{-1} reflect the existence of CN groups, indicating that the successful formation of the IL-POM hybrids via strong ionic bond interactions.

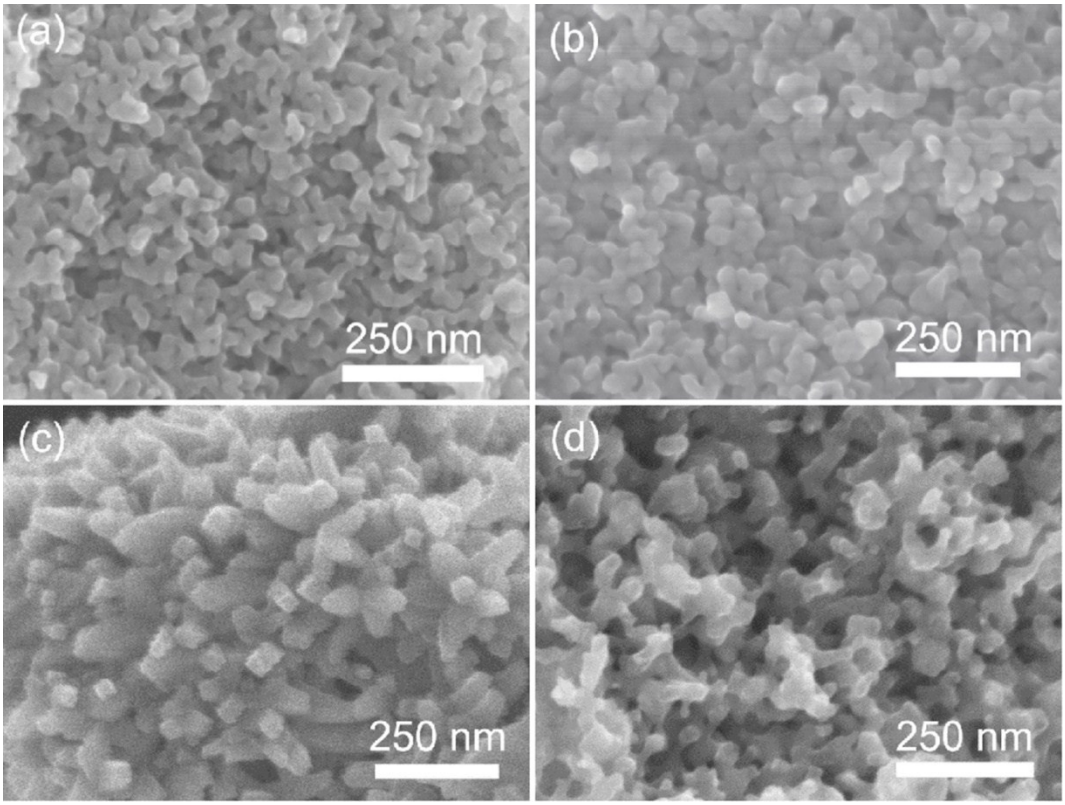

Fig. S5 SEM images of (a) D[3-CNBzBPy]$_{1.5}$PMo, (b) D[BzBPy]$_{1.5}$PMo, (c) N/P-Mo_2C@C3 and (d) N/P-MoO_2@C0.

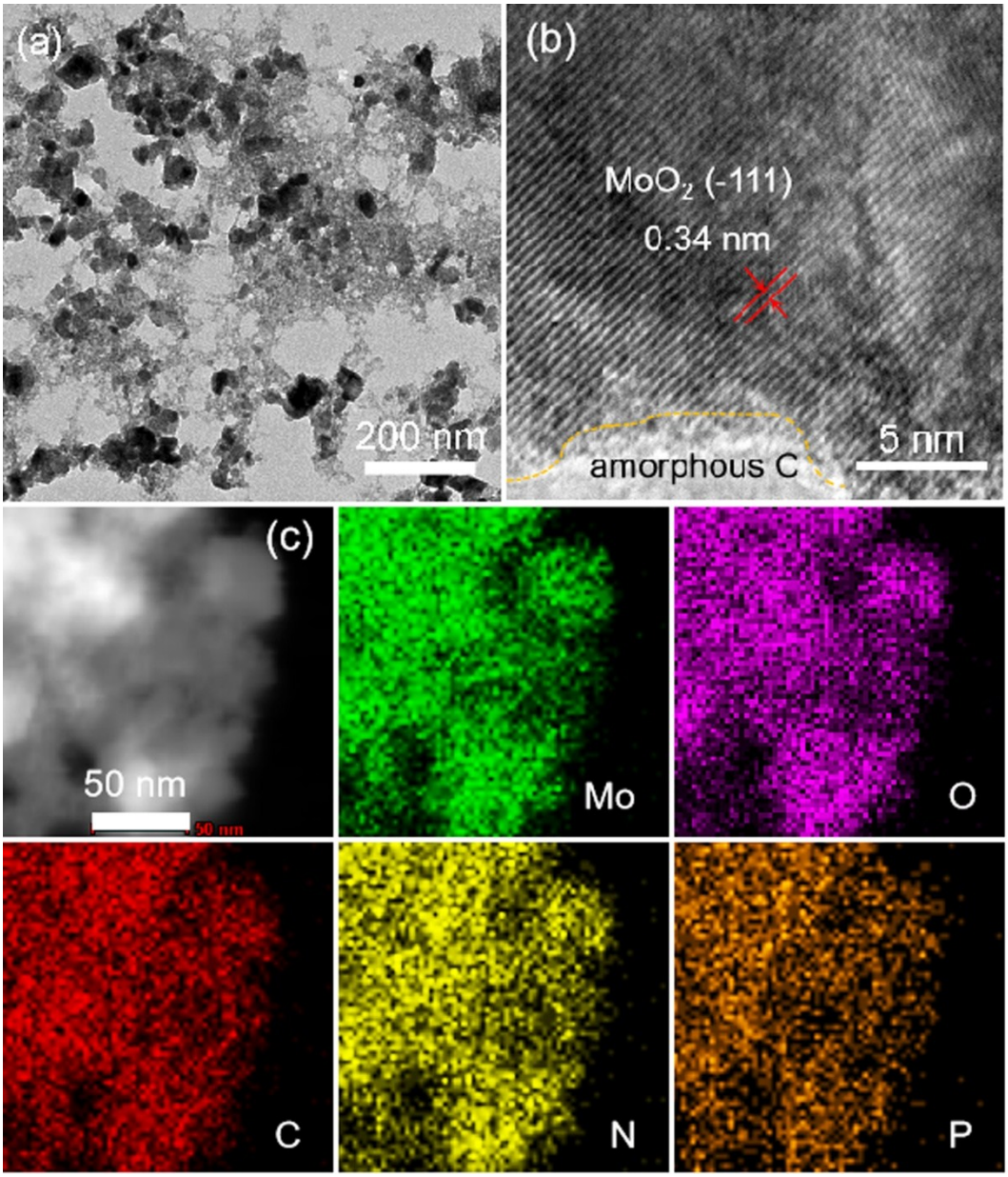

Fig. S6 (a) TEM image and (b) HR-TEM image of N/P-MoO_2@C0. (c) STEM EDS elemental mapping of Mo, O, C, N and P in the N/P-MoO_2@C0 at the nanoscale (50 nm).

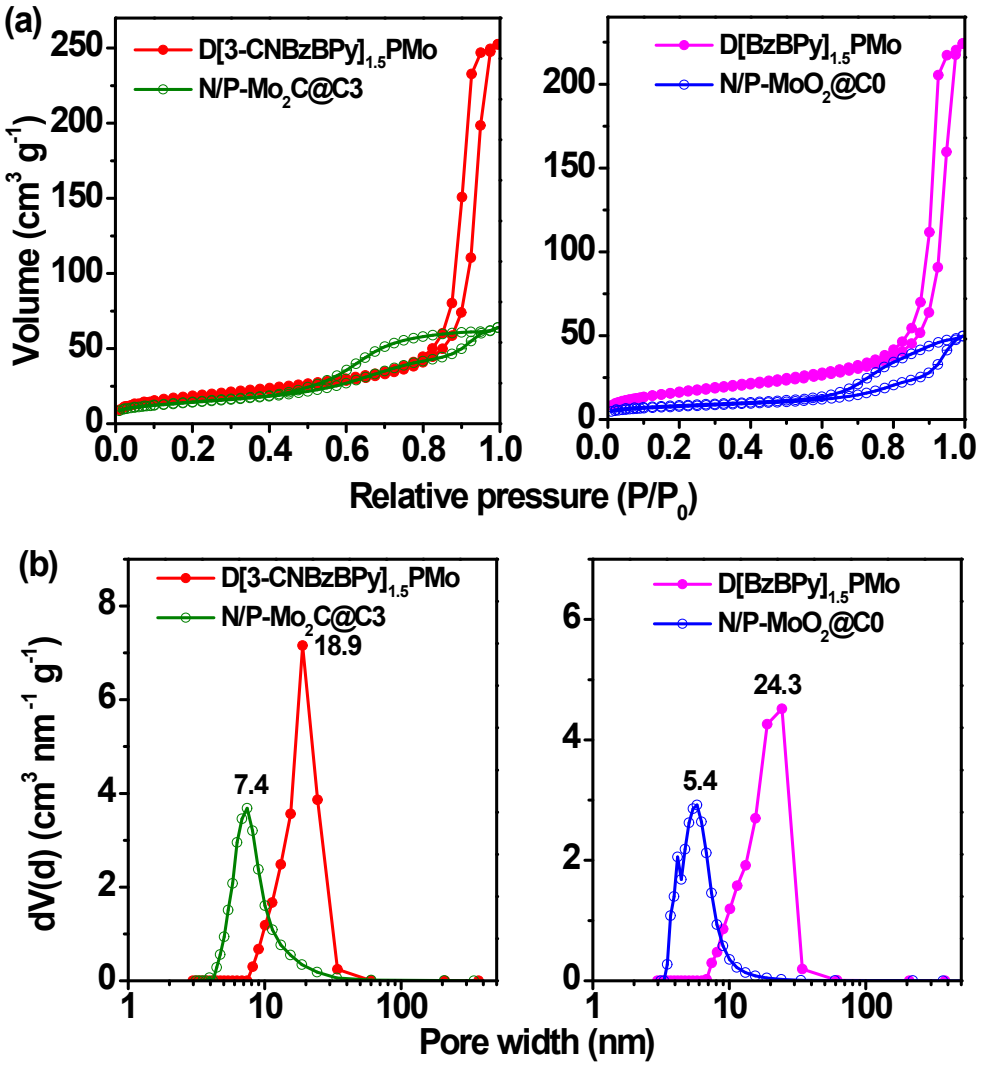

Fig. S7 (a) N_2 adsorption-desorption isotherms and (b) BJH pore size distributions of IL-POMs and their derived materials.

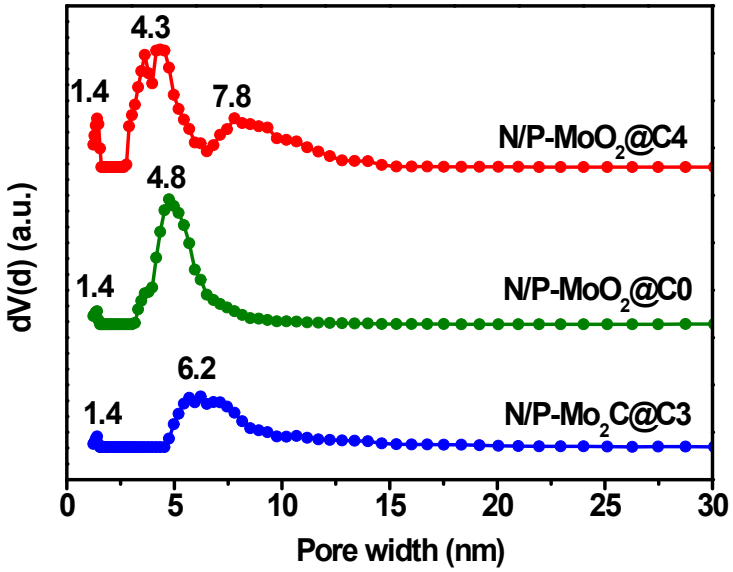

Fig. S8 Pore size distributions of N/P-MoO_2@C4, N/P-MoO_2@C0 and N/P-Mo_2C@C3 calculated by the non-local density function theory (NLDFT).

In addition, pore size distributions of N/P-MoO_2@C4, N/P-MoO_2@C0 and N/P-Mo_2C@C3 were also calculated by the non-local density function theory (NLDFT). As shown in Fig. S8, a small amount of micropores centred at 1.4 nm appear in the final N/P-MoO_2@C networks, which is consistent with the results of micropore surface areas (Table S1). The mesopore size distributions described in Fig. S8 have the similar trend with the BJH pore size distributions (Fig. 1g and Fig. S7b).

Table S1 The textural properties of mesoporous IL-POMs and derived N/P-MoO_2 (or Mo_2C) @C networks.

Sample	S_{BET} (m^2 g^{-1}) [a]	S_{micro} (m^2 g^{-1}) [b]	V_{total} (cm^3 g^{-1}) [c]	D_p (nm) [d]
D[4-CNBzBPy]$_{1.5}$PMo	63	11.3	0.37	19.0
D[BzBPy]$_{1.5}$PMo	60	10.7	0.35	24.3
D[3-CNBzBPy]$_{1.5}$PMo	65	10.2	0.39	18.9
N/P-MoO_2@C4	89	7.8	0.16	3.5
N/P-MoO_2@C0	51	4.6	0.10	5.4
N/P-Mo_2C@C3 [e]	28	2.7	0.08	7.5

[a] Surface area calculated using the BET method. [b] Micropore surface area calculated by *t*-plot method. [c] The total pore volume at P/P_0=0.99. [d] The most probable pore diameter calculated by the BJH method. [e] N/P-Mo_2C@C3 was prepared by the pyrolysis of D[3-CNBzBPy]$_{1.5}$PMo under the same conditions.

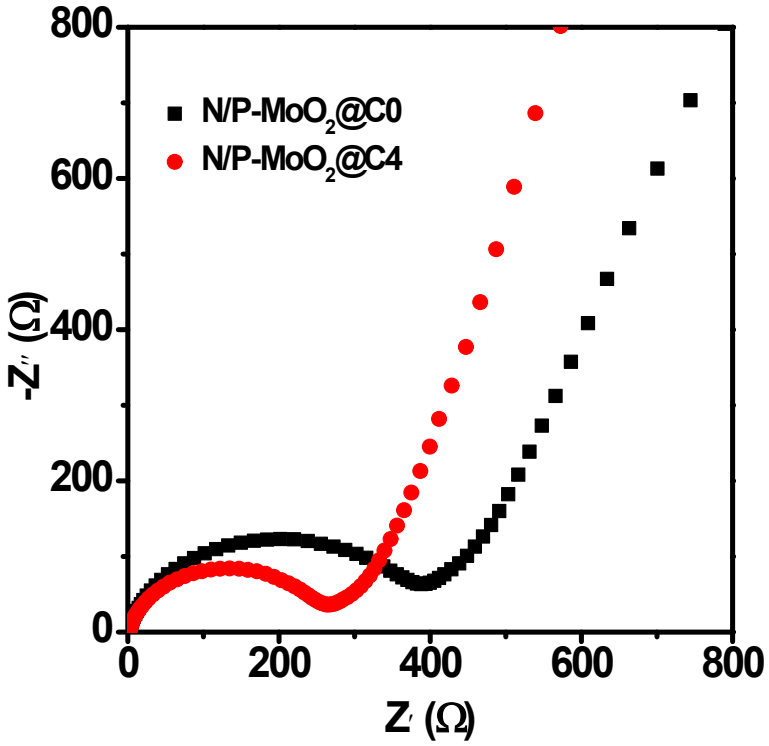

Fig. S9 Nyquist plot of the N/P-MoO_2@C0 and N/P-MoO_2@C4.

The depressed semicircle in Fig. S9 is related to charger transfer resistance of electrode (R_{ct}). Apparently, the N/P-MoO_2@C4 shows a lower R_{ct}, which will contribute to faster ion/electron transportation. The tightly-packed 3D sponge-like morphology of N/P-MoO_2@C4 not only provide ion/electron with multiply channels for transportation, but also shorten the transport distance.

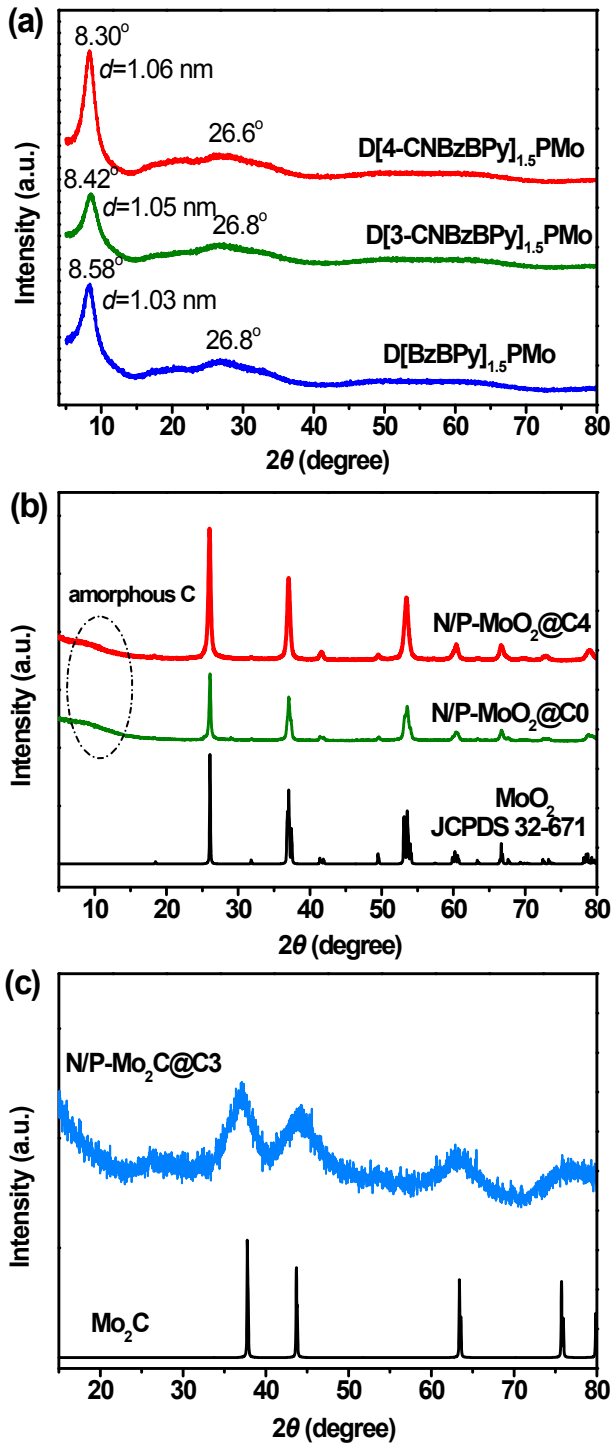

Fig. S10 XRD patterns of (a) IL-POM precursors D[4-CNBzBpy]$_{1.5}$PMo, D[3-CNBzBpy]$_{1.5}$PMo, and D[BzBpy]$_{1.5}$PMo. (b) N/P-MoO$_2$@C4 and N/P-MoO$_2$@C0. (c) N/P-Mo$_2$C@C3.

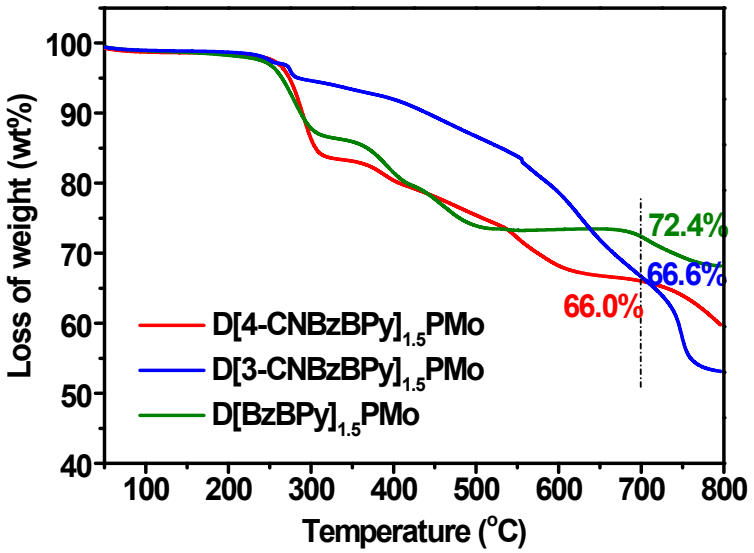

Fig. S11 TGA cures of D[4-CNBzBpy]$_{1.5}$PMo, D[3-CNBzBpy]$_{1.5}$PMo and D[BzBpy]$_{1.5}$PMo in N_2.

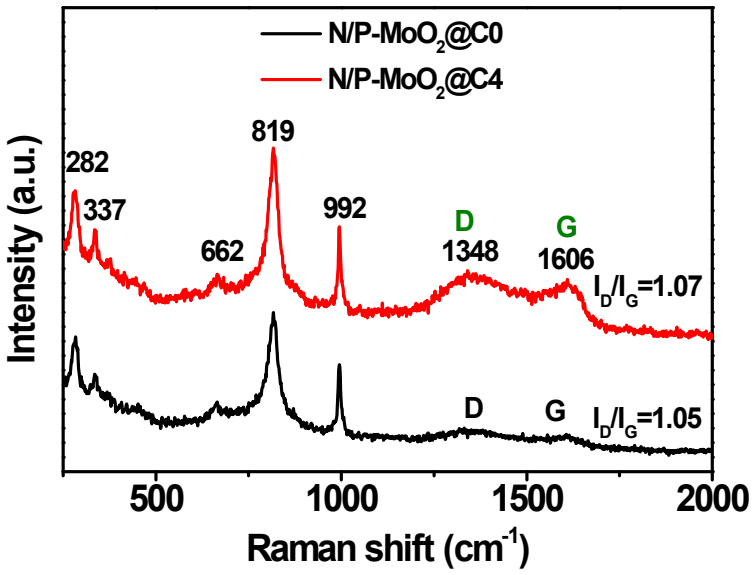

Fig. S12 Raman spectra for N/P-MoO_2@C0 and N/P-MoO_2@C4.

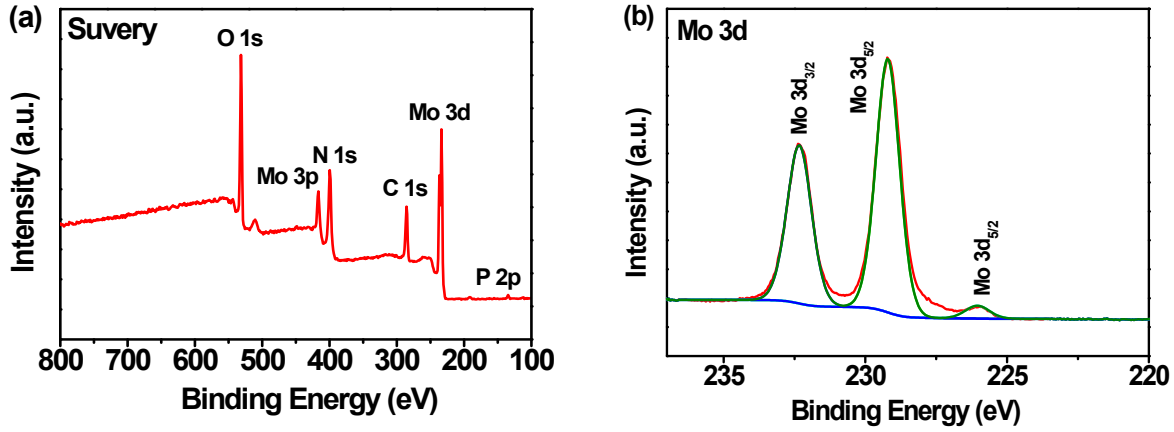

Fig. S13 (a) Wide-scan survey XPS spectrum of N/P-MoO_2@C4. (b) Mo 3d XPS spectra.

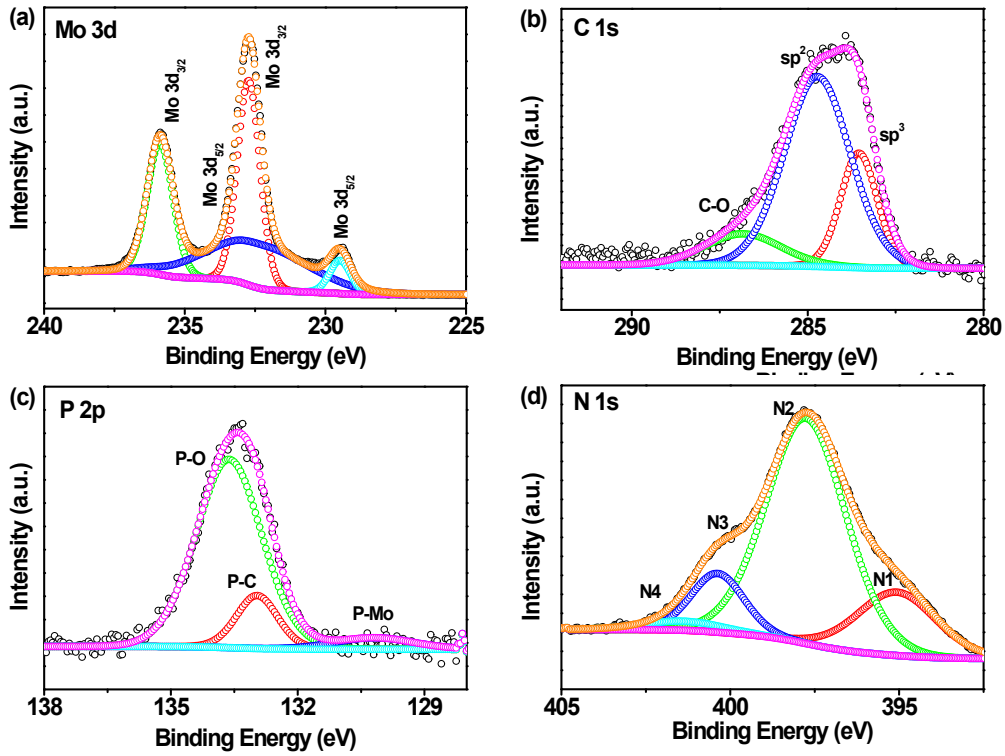

Fig. S14 High-resolution XPS spectra of (a) Mo 3d, (b) N 1s, (c) C 1s and (d) P 2p of N/P-MoO_2@C0.

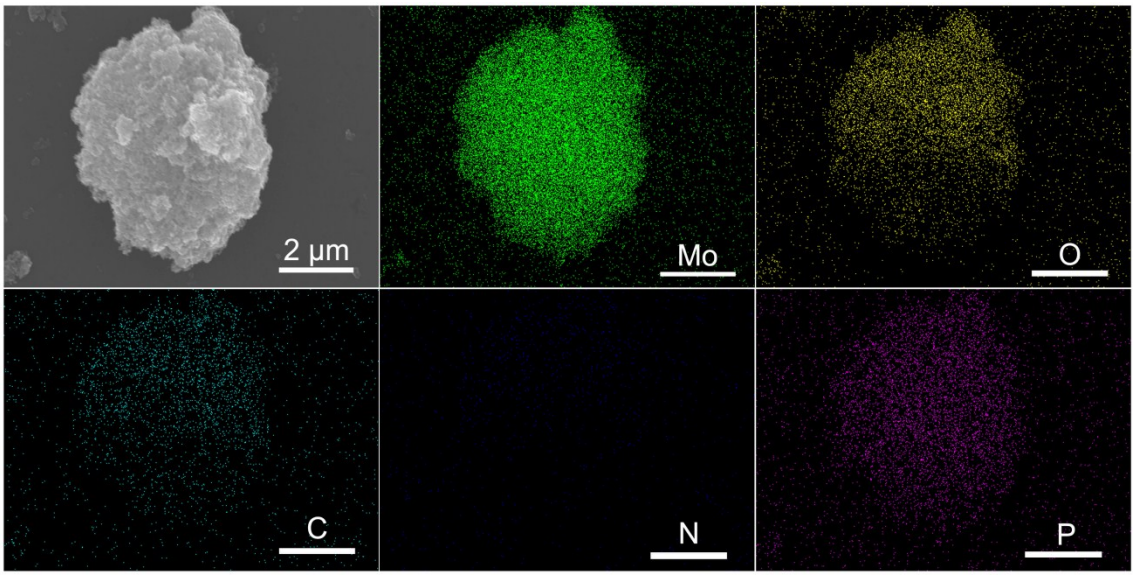

Fig. S15 SEM EDS mapping images of N/P-MoO_2@C4 for the elements Mo, O, C, N and P at the micrometer scale.

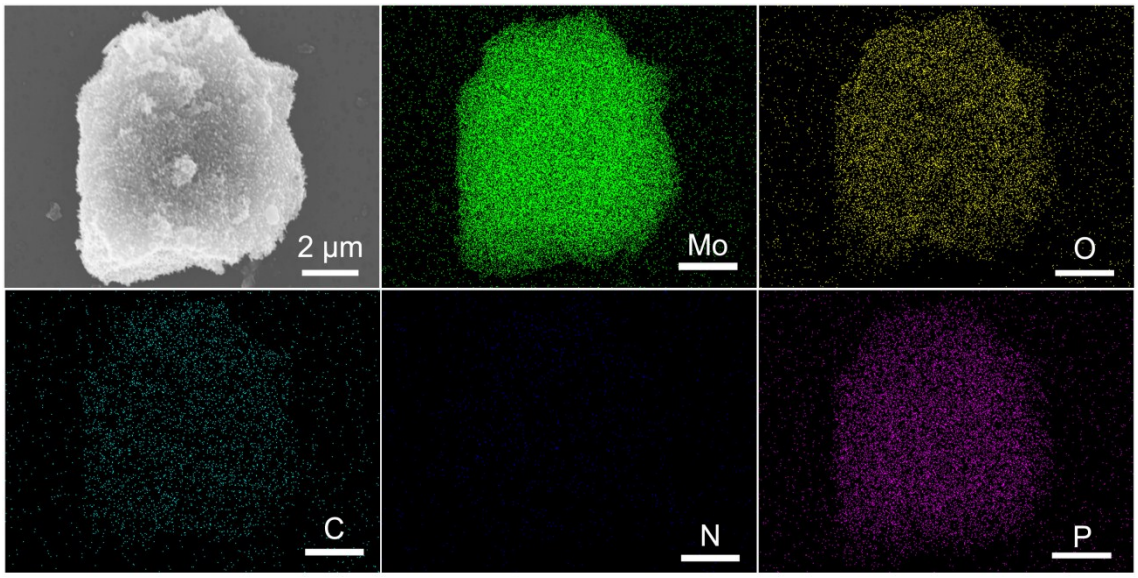

Fig. S16 SEM EDS mapping images of N/P-MoO_2@C0 for the elements Mo, O, C, N and P at the micrometer scale.

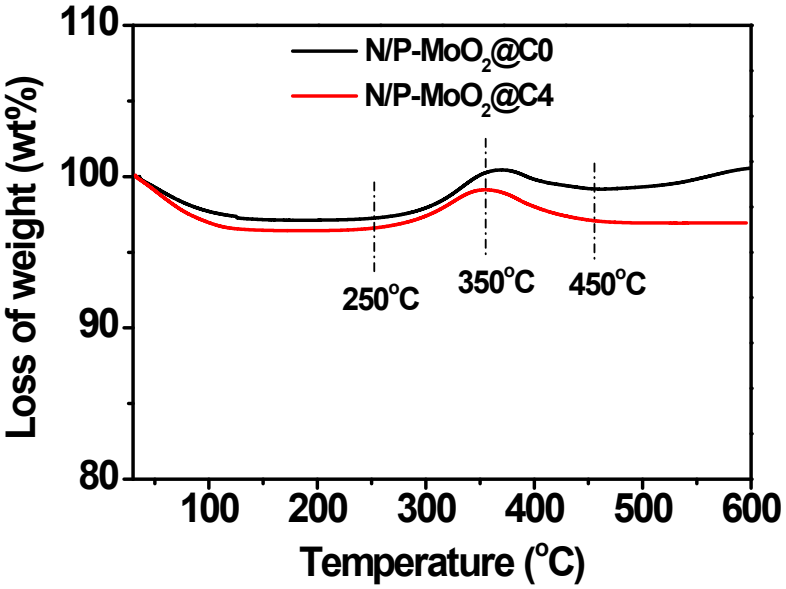

Fig. S17 TGA cures of N/P-MoO_2@C0 and N/P-MoO_2@C4 in air.

As shown in Fig. S17, the slight weight loss before 220 °C is likely caused by desorption of water or gas molecules. The successive weight gain and loss between 250-450 °C is caused by the simultaneous oxidation of MoO_2 to MoO_3 and the combustion of carbon, nitrogen and phosphorus under an air atmosphere.

Table S2 Elemental compositions of N/P-MoO_2@C0 and N/P-MoO_2@C4.

Sample	MoO_2 (wt%)[a]	C (wt%)[b]	N (wt%)[b]	P (wt%)[c]
N/P-MoO_2@C4	86.1	5.2	1.8	6.9
N/P-MoO_2@C0	88.2	3.9	1.1	6.8

[a] The content of MoO_2 is calculated based on the TGA results collected in air. [b] The C and N content in each sample is obtained based on elemental analysis. [c] The P content is calculated based on (100-wt_{MoO2}-wt_C-wt_N)%.

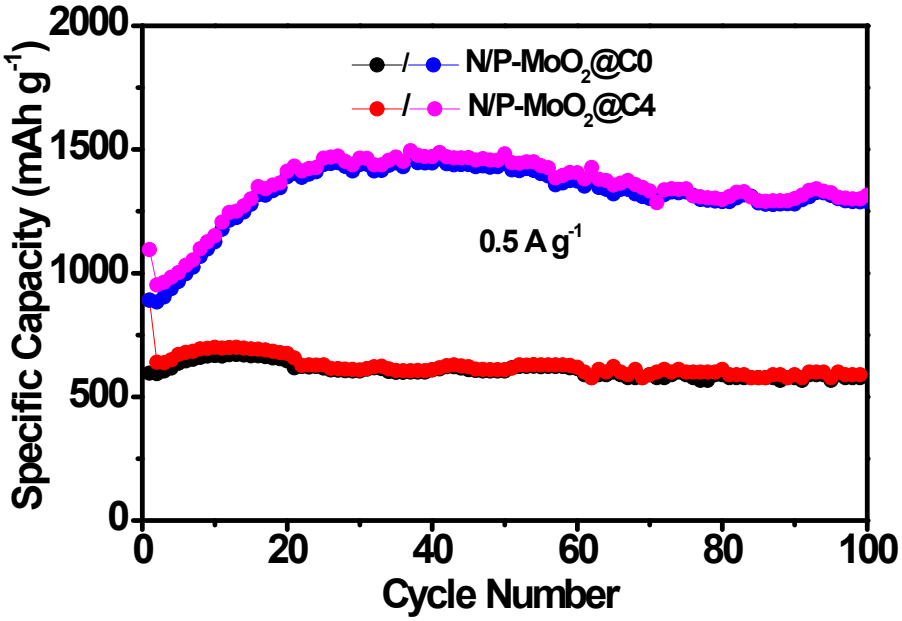

Fig. S18 Cycling performance of N/P-MoO_2@C0 and N/P-MoO_2@C4 at 0.5 A g^{-1}.

Table S3. Comparisons of lithium storage performance of different MoO_2-based and other Mo-based electrodes.

Samples	Current density ($A\ g^{-1}$)	Capacity ($mAh\ g^{-1}$)	Cycle	Ref.
Triple shelled MoO_2/C	0.5	580	200	S1
Mesoporous carbon-MoO_2	0.084	581	30	S2
MoO_2-Graphene	1.0	600	70	S3
MoO_2@N-doped carbon	0.5	700	100	S4
3D MoO_2	1.0	650	100	S5
Ultrathin 2D MoO_2	1.0	489	1050	S6
MoO_2/C	1.6	650	1000	S7
MoO_2 flowers on graphene	0.38	477.2	100	S8
MoO_2@C nanorod	10	312	268	S9
MoO_2-N,S doped graphene	0.2	1250	100	S10
MoS_2-graphene sheet	0.1	1077	150	S11
Freestanding MoO_2/Mo_2C	0.1	1103	50	S12
MoS_2-MoO_2	10	295	300	S13
Core-shell TiO_2@MoO_2	0.5	390	450	S14
TiO_2@MoO_2-C	10	60	1000	S15
MoS_2-$MoSe_2$	0.2	676	200	S16
MoS_2@CNT	0.2	747	200	S17
MoS_2-rGO/HCS	2.0	753	1000	S18
Mo_xC@N-C	0.5	521	200	S19
TiO_2@NC@MoS_2	1.0	590	200	S20
N/P-MoO_2@C4	0.5	1381	100	This work
	20	346	5000	

Reference

[S1] Y. Wang, L. Yu and X. W. Lou, *Angew. Chem. Int. Ed*., 2016, **55**, 14668-14672.

[S2] Y. Zhou, I. Lee, C. W. Lee, H. S. Park, H. Son and S. Yoon, *B. Korean Chem. Soc.,* 2014, **35**, 257-260.

[S3] Y. Sun, X. Hu, W. Luo and Y. Huang, *ACS Nano*, 2011, **5**, 7100-7107.

[S4] X. Tan, C. Cui, S. Wu, B. Qiu, L. Wang and J. Zhang, *Chem. Asian J.,* 2017, **12**, 36-40.

[S5] G. Xu, P. Liu, Y. Ren, X. Huang, Z. Peng, Y. Tang and H. Wang, *J. Power Sources,* 2017, **361**, 1-8.

[S6] C. Xia, Y. Zhou, D. B. Velusamy, A. A. Farah, P. Li, Q. Jiang, I. N. Odeh, Z. Wang, X. Zhang and H. N. Alshareef, *Nano Lett.,* 2018, **18**, 1506-1515.

[S7] L. Chen, H. Jiang, H. Jiang, H. Zhang, S. Guo, Y. Hu and C. Li, *Adv. Energy Mater.,* 2017, **7**, 1602782.

[S8] Y. Zhou, H. Xie, C. Wang, Q. He, Q. Liu, Z. Muhammad, Y. A. Hgeem, Y. Sang, S. Chen and L. Song, *J. Phys. Chem. C,* 2017, **121**, 15589-15596.

[S9] Y. Wang, Z. Huang and Y. Wang, *J. Mater. Chem. A,* 2015, **3**, 21314-21320.

[S10] J. Pei, H. Geng, H. Ang, L. Zhang, H. Wei, X. Cao, J. Zheng and H. Gu, *Nanotechnology,* 2018, **29**, 295404.

[S11] Y. Teng, H. Zhao, Z. Zhang, Z. Li, Q. Xia, Y. Zhang, L. Zhao, X. Du, Z. Du, P. Lv and K. Świerczek, *ACS Nano,* 2016, **10**, 8526-8535.

[S12] H. Li, H. Ye, Z. Xu, C. Wang, J. Yin and H. Zhu, *Phys. Chem. Chem. Phys.,* 2017, **19**, 2908-2914.

[S13] D. Xiao, J. Zhang, X. Li, D. Zhao, H. Huang, J. Huang, D. Cao, Z. Li and C. Niu, *ACS Nano,* 2016, **10**, 9509-9515.

[S14] S. Wang, Z. Zhang, Y. Yang and Z. Tang, *ACS Appl. Mater. Interfaces,* 2017, **9**, 23741-23747.

[S15] C. Zhao, C. Yu, M. Zhang, H. Huang, S. Li, X. Han, Z. Liu, J. Yang, W. Xiao, J. Liang, X. Sun and J. Qiu, *Adv. Energy Mater.,* 2017, **7**, 1602880.

[S16] J. Yang, J. Zhu, J. Xu, C. Zhang and T. Liu, *ACS Appl. Mater. Interfaces,* 2017, **9**, 44550-44559.

[S17] H. Zhou, R. Zhang, S. Song, C. Xiao, G. Gao and S. Ding, *ACS Appl. Energy Mater.,* 2018, **1**, 5112-5118.

[S18] X. Hu, Y. Li, G. Zeng, J. Jia, H. Zhan and Z. Wen, *ACS Nano,* 2018, **12**, 1592-1602.

[S19] S. Liu, F. Li, D. Wang, C. Huang, Y. Zhao, J.-B. Baek and J. Xu, *Small Meth.,* 2018, **2**, 1800040.

[S20] S. Wang, B. Y. Guan, L. Yu and X. W. Lou, *Adv. Mater.,* 2017, **29**, 1702724.